Meas. Sci. Technol. **19** (2008) 075204 (8pp) doi:10.1088/0957-0233/19/7/075204

Alternating current potential-drop measurement of the depth of case hardening in steel rods

John R Bowler, Yongqiang Huang, Haiyan Sun, Jonathan Brown and Nicola Bowler

Iowa State University, Center for Nondestructive Evaluation, Applied Sciences Complex II, 1915 Scholl Road, Ames, IA 50011, USA

Received 14 January 2008, in final form 6 May 2008
Published 12 June 2008
Online at stacks.iop.org/MST/19/075204

Abstract
The case depth of induction-hardened steel rods has been determined using multi-frequency alternating current potential-drop measurements. Experimental results are analyzed using a model which approximates the variation in the material properties of a hardened rod by assuming that a homogeneous core is surrounded by a homogeneous case-hardened layer of uniform thickness. Experimental measurements on an untreated rod are used to estimate the core conductivity and permeability of similar hardened rods. The implicit assumption is that the material parameters in the core region are unchanged in the hardening process. The case depth is found by parameter fitting to minimize a penalty function representing the overall difference between multi-frequency potential-drop measurements and theoretical predictions. Case-depth values found nondestructively show reasonable agreement with those found using Rockwell hardness measurements on sectioned rods.

Keywords: steel rod, depth of case hardening, alternating current potential drop

(Some figures in this article are in colour only in the electronic version)

1. Introduction

Case hardening of steel components improves the resistance to wear by changing the microstructure or by changing both the microstructure and the chemical composition of the surface region usually by adding carbon. Because of the high cost, inconvenience and resources needed for direct destructive measurements, a number of nondestructive methods have been investigated to infer hardness and case depth from test data. The methods examined have used isotopic radiation [1], ultrasonic waves [2, 3], electromagnetic fields, thermal techniques [4, 5] and direct-current potential-drop measurements [6].

Several electromagnetic methods, such as eddy currents [7, 8] or Barkhausen noise measurement [9] give indications that can be correlated with hardness. The question this raises is how best to take advantage of the observations. A traditional approach is to establish empirically a calibration curve that relates a measured physical quantity with the hardness. For example, it has been shown that there is a strong correlation between hardness and magnetic coercivity and, to a lesser extent, initial permeability [10]. Since one type of measurement alone does not provide all the information needed, a natural development is to measure several different quantities and infer the hardness and possibly the case depth from the data using a multi-variant regression analysis [11].

Here, an alternative approach is presented in which the material properties, conductivity and initial permeability are found together with the case depth using a model of the measurement process based on linear field theory. The initial permeability can be used to give an estimate of hardness but we have not done this. Instead we have focused on the more challenging problem of estimating the case depth without relying on calibration data. The aim is to find an approach that can tolerate changes in the raw materials and the manufacturing environment without the need for re-calibration.

We model cylindrical case-hardened steel rods as uniform in the axial direction having a homogeneous substrate

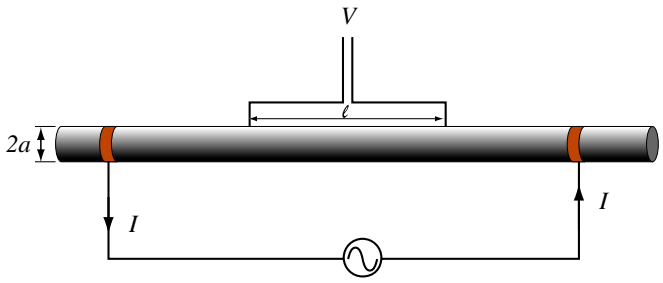

Figure 1. Schematic diagram of the ACPD measurement system. Alternating current I is applied to the rod by circular copper bands, clamped to the rod. Potential drop V is measured by a lock-in amplifier with high impedance.

surrounded by a homogeneous surface layer of uniform thickness. An axially-symmetric alternating electrical current is passed down a rod and measurements of potential drop made at a number of frequencies, spanning two decades or more. The data are interpreted using a theoretical description of the field in the rod. The elementary theory of the electromagnetic field in a homogeneous rod is described first, from which predictions of the alternating current potential drop (ACPD) may be made for a given conductivity and permeability. Then the ACPD for a case-hardened steel rod is evaluated according to the stated assumptions. The method is applied to estimate the depth of case hardening in three SAE/AISI 1045 steel rods with nominal case depths 1.0, 1.5 and 2.0 mm. Good agreement is achieved between estimated values and those from destructive microhardness measurements.

2. ACPD for a homogeneous cylindrical rod

Consider an axially-symmetric alternating current flowing through a long cylindrical rod, figure 1. The rod has radius a, conductivity σ and absolute permeability μ which is assumed to be a linear, frequency-independent parameter. The current varies sinusoidally with time as the real part of $e^{j\omega t}$. Due to the axial symmetry, and by neglecting end effects, the complex amplitude of the electric field $\mathbf{E}$ is a function of radial coordinate ρ only. Then $\mathbf{E} = \hat{z}E(\rho)$, where $\hat{z}$ is a unit vector in the direction of the rod axis. The field satisfies

$$\frac{d^2E}{d\rho^2} + \frac{1}{\rho}\frac{dE}{d\rho} + k^2E = 0, \tag{1}$$

where $k^2 = -j\omega\mu\sigma$. This is Bessel's equation for zero-order Bessel functions. A solution that is finite as $\rho \to 0$ is given by

$$E(\rho, k) = E_0(k)\frac{J_0(k\rho)}{J_0(ka)}, \tag{2}$$

where $E_0(k) = E(0, k)$ is the electric field intensity on the rod surface and the $J_\nu(x)$ are Bessel functions of the first kind. The surface field can be related to the current, a measured quantity, by noting that the total current passing through the rod is

$$I = 2\pi\sigma\int_0^a E(\rho, k)\rho\, d\rho. \tag{3}$$

Using equation (2), evaluation of the integral in (3) and rearranging gives

$$E_0(k) = \frac{I}{2\pi\sigma}\frac{k}{a}\frac{J_0(ka)}{J_1(ka)}. \tag{4}$$

Letting ℓ be the distance between the two voltage contact points, which are placed on a line parallel with the rod axis, the potential difference between these points is given by

$$V = E_0(k)\ell = \frac{I}{2\pi\sigma}\frac{k\ell}{a}\frac{J_0(ka)}{J_1(ka)}. \tag{5}$$

In addition to this potential-drop term, the measured voltage includes a contribution from the electromotance due to a changing magnetic flux linking the measurement circuit. Expressing the induced electromotance in terms of the self-inductance L_0, the total voltage sensed across a length ℓ of the rod is

$$V_T = \frac{I}{2\pi\sigma}\frac{k\ell}{a}\frac{J_0(ka)}{J_1(ka)} + j\omega I L_0. \tag{6}$$

Equation (6) can be used to estimate linear material properties, conductivity and permeability of a homogeneous rod from multi-frequency measurements of potential drop.

At low frequencies, where the electromagnetic skin depth $\delta = \sqrt{2/(\omega\mu\sigma)}$ is much greater than the rod diameter, the argument of the Bessel functions is small. This means that V of equation (5) may be approximated by a few terms in the following series, obtained by manipulating the ascending series expansion for Bessel functions of the first kind given in reference [12], equation (9.1.10),

$$\frac{z}{2}\frac{J_0(z)}{J_1(z)} \approx 1 - \frac{z^2}{8} - \frac{z^4}{192} - \frac{z^6}{3072} - \cdots \tag{7}$$

Rewriting (5) in terms of the rod impedance per unit length,

$$Z(\omega) = \frac{V}{\ell I} = R + j\omega L, \tag{8}$$

the small-argument expansion gives

$$\begin{aligned} R &\approx \frac{1}{\pi a^2\sigma}\left(1 + \frac{a^2}{48\delta^2} + \cdots\right) \\ L &\approx \frac{\mu}{8\pi}\left(1 + \frac{a^2}{96\delta^2} + \cdots\right). \end{aligned} \tag{9}$$

Thus, R initially increases linearly with frequency from its dc value which is independent of permeability. The leading term in the expansion for the inductive component is proportional to permeability and independent of conductivity. Hence from the real and imaginary parts of the complex ACPD at low frequency, it is possible to determine both the conductivity and permeability of the rod. In fact, we determine the permeability and conductivity by a fitting process using (6) but the above expression for the low-frequency impedance limit provides a useful check on the results.

It is also useful to define a bounding frequency for the quasi-static regime, f_s, below which V is essentially real and constant. Write the expression for R, relation (9), as follows:

$$R \approx \frac{1}{\pi a^2\sigma} + \frac{f\mu}{48} + \cdots. \tag{10}$$

Then define f_s to be the frequency at which the magnitude of the term of order f^1 in equation (10) is 1/100 of the magnitude of the term of order f^0. This gives

$$f_s = \frac{48}{100\pi a^2 \sigma \mu} \approx \frac{1}{2\pi a^2 \sigma \mu}. \tag{11}$$

Equation (11) reveals that f_s is inversely proportional to the cross-sectional area, the conductivity and the permeability of the rod.

3. Voltage measured on case-hardened steel rods

We next consider a hardened steel rod with radius a, having a conductivity of σ_1 and permeability of μ_1 in its core ($\rho \leqslant c$). Let the complex amplitude of the electric field in the core be $E_1(\rho)$. In its outer layer ($c \leqslant \rho \leqslant a$), the conductivity and permeability are σ_2 and μ_2 respectively and the electric field has a complex amplitude $E_2(\rho)$. Both μ_1 and μ_2 are assumed to be linear, frequency-independent parameters. Passing an alternating current through a hardened steel rod in the axial direction gives rise to an electric field intensity governed by

$$\frac{\mathrm{d}^2 E_i}{\mathrm{d}\rho^2} + \frac{1}{\rho}\frac{\mathrm{d}E_i}{\mathrm{d}\rho} + k_i^2 E = 0, \tag{12}$$

where $k_i = -\mathrm{j}\omega\mu_i\sigma_i$ with $i = 1, 2$. The solution of (12) can be written as

$$E_1(\rho) = E_0(k_1, k_2) A J_0(k_1\rho) \tag{13}$$

and

$$E_2(\rho) = E_0(k_1, k_2)[B J_0(k_2\rho) + C Y_0(k_2\rho)], \tag{14}$$

where the Y_ν are Bessel functions of the second kind and A, B and C are scaling factors to be determined by boundary and interface conditions.

For the first condition we fix the electric field intensity on the rod surface E_0, which means that $E_2(a) = E_0(k_1, k_2)$. This gives

$$B J_0(k_2 a) + C Y_0(k_2 a) = 1. \tag{15}$$

Next, we use the fact that the tangential electric field is continuous at $\rho = c$ to give the second condition

$$B J_0(k_2 a) + C Y_0(k_2 a) = A J_0(k_1 a). \tag{16}$$

Third, the continuity of the tangential magnetic field is used. Faraday's induction law, $\nabla \times \mathbf{E} = -\mathrm{j}\omega\mu\mathbf{H}$, shows that $\mathrm{j}\omega H_\phi = (1/\mu)\,\mathrm{d}E/\mathrm{d}\rho$ in this case. Therefore we apply the continuity condition

$$\frac{1}{\mu_1}\frac{\mathrm{d}E_1}{\mathrm{d}\rho} = \frac{1}{\mu_2}\frac{\mathrm{d}E_2}{\mathrm{d}\rho} \tag{17}$$

to the electric field at $\rho = c$ to give the third condition

$$A\mu_2 k_1 J_1(k_1 c) = B\mu_1 k_2 J_1(k_2 c) + C\mu_1 k_2 Y_1(k_2 c). \tag{18}$$

The coefficients A, B, C can be determined from a 3×3 matrix equation formed from (15), (16) and (18). Using the co-factors

$$\Delta_A = \mu_1 k_2 [J_1(k_2 c) Y_0(k_2 c) - Y_1(k_2 c) J_0(k_2 c)] = \frac{2\mu_1}{\pi c} \tag{19}$$

$$\Delta_B = \mu_2 k_1 J_1(k_1 c) Y_0(k_2 c) - \mu_1 k_2 J_0(k_1 c) Y_1(k_2 c) \tag{20}$$

$$\Delta_C = \mu_1 k_2 J_0(k_1 c) J_1(k_2 c) - \mu_2 k_1 J_1(k_1 c) J_0(k_2 c) \tag{21}$$

and the determinant

$$\begin{aligned}\Delta &= J_0(k_2 a)\,[\mu_2 k_1 J_1(k_1 c) Y_0(k_2 c) - \mu_1 k_2 J_0(k_1 c) Y_1(k_2 c)] \\ &\quad + Y_0(k_2 a)\,[\mu_1 k_2 J_0(k_1 c) J_1(k_2 c) - \mu_2 k_1 J_1(k_1 c) J_0(k_2 c)] \\ &= J_0(k_2 a)\Delta_B + Y_0(k_2 a)\Delta_C,\end{aligned} \tag{22}$$

we obtain

$$A = \Delta_A/\Delta,\ B = \Delta_B/\Delta, C = \Delta_C/\Delta. \tag{23}$$

With the scaling coefficients A, B and C now known, the electric field intensity inside the rod can be found from equations (13) and (14). It is now straightforward to determine an expression for the ACPD of the hardened rod from the relation

$$V = E_0(k_1, k_2)\ell = E_2(a)\ell. \tag{24}$$

In order to evaluate (24), the surface field $E_0(k_1, k_2)$ is now written in terms of the current in the rod, I, which is a measured quantity. In the layered rod, I can be written as

$$I = 2\pi\sigma_1 \int_0^c E_1(\rho)\rho\,\mathrm{d}\rho + 2\pi\sigma_2 \int_c^a E_2(\rho)\rho\,\mathrm{d}\rho. \tag{25}$$

From (13) and (14), and the following integral [12], equation 11.3.24,

$$\int_0^c x Y_0(x)\,\mathrm{d}x = cY_1(c) + \frac{2}{\pi} \tag{26}$$

equation (25) becomes

$$\begin{aligned}\frac{I}{E_0} &= 2\pi\sigma_1 A c J_1(k_1 c)/k_1 + 2\pi\sigma_2 B[a J_1(k_2 a) - c J_1(k_2 c)]/k_2 \\ &\quad + 2\pi\sigma_2 C[a Y_1(k_2 a) - c Y_1(k_2 c)]/k_2.\end{aligned} \tag{27}$$

Thus the potential drop, including electromotance in the loop of the pick-up circuit, is

$$V_T = E_0\ell + \mathrm{j}\omega I L_0, \tag{28}$$

where ℓ is again the length measured along the rod between the two contact points, and E_0 is given by (27) with (19) to (23). Equation (28) and (27) gives the relationship between the rod parameters and the measured voltage–frequency curve. Hence, by fitting multi-frequency ACPD data to theoretical predictions, the parameters of a layered rod can be estimated.

4. Experiment

4.1. ACPD measurement method

ACPD measurements have been made for a range of frequencies from 1 Hz to 10 kHz using a lock-in amplifier. The quality of the results depends on the ability to measure small values of V accurately and on ensuring that the field is axially symmetric at the rod. In order to ensure axial symmetry, the rod is placed coaxially in a 10 cm diameter copper tube, figure 2, which provides a return path for the current. This reduces the measurement dependence on the layout of the current-carrying cables. An alternating current of approximately 1 A is passed through the rod during a measurement, giving a potential drop of a few tens to a few hundred microvolts, recorded by a lock-in amplifier,

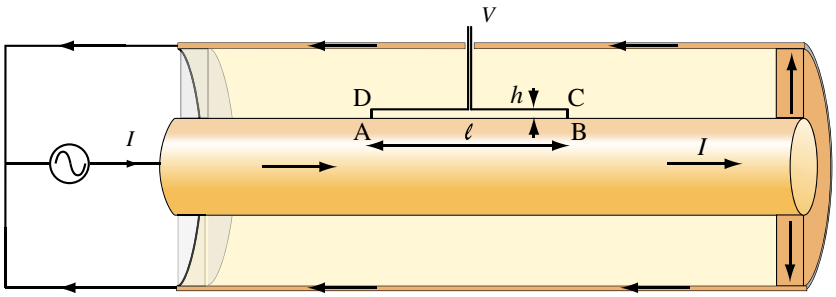

Figure 2. Co-axial measurement system with the rod supported at one end of a copper tube by a polymethylmethacrylate (perspex) ring at one end and a brass ring at the other to provide a conducting path to the tube. The voltage contacts at A and B are shown as wired at a height $h = \mathrm{AD} = \mathrm{BC}$ from the surface of the rod. This height is kept small in order to limit the self-inductance in the pick-up loop.

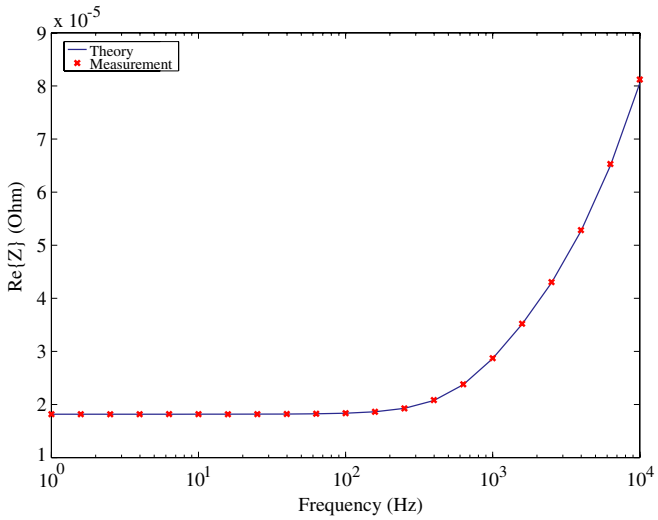

Figure 3. Comparison between theory and experiment of the real part of the rod impedance measured on a homogeneous copper rod.

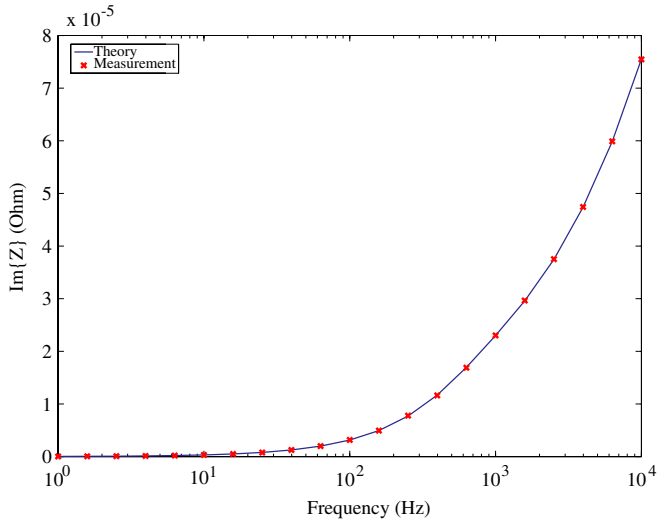

Figure 4. As for figure 3 but for the imaginary part of the impedance.

depending on the frequency and rod parameters. The phase and amplitude of the current was determined from the voltage drop across a precision series resistor also measured using the lock-in amplifier.

Figures 3 and 4 show the comparison between theory and experiment for a copper rod, diameter 11 mm, used as a test sample. The conductivity of the copper, found by fitting to the real part of the rod impedance data, is 58.2 MS m^{-1} (100.3% IACS). This indicates relative uncertainty in the conductivity measurement of less than 0.01, since the conductivity of annealed copper is around 100 or 101% IACS, depending on the material grade. Data from the experiment on the copper rod was also used to find the self-inductance of the measurement circuit. This was determined to be 480 ± 20 pH for contact points located 15.4 ± 0.1 cm apart. Connection wires attached to the voltage contacts are laid close to the surface of the rod and wound together from the mid-point as a twisted pair to minimize self-induction. If the connecting wires are assumed to be located, on average, a distance h from the surface of the rod and if self-induction in the twisted pair can be neglected, then it is easy to show by integrating the rate of change of the magnetic flux in air $B_\phi = \mu_0 I/2\pi\rho$ over the pick-up loop that

$$L_0 = \frac{\mu_0 \ell}{2\pi} \log\left(1 + \frac{h}{a}\right). \tag{29}$$

Using this formula, a self-inductance of 480 pH leads to a value of approximately 170 μm for h. Because the potential drop is relatively large, the self-inductance can often be neglected, depending on the upper frequency used, but in fact we routinely apply the correction indicated in equation (28) for the induced electromotance, based on the value of self-inductance determined here.

From equation (11) the value of the frequency at which $\mathrm{Re}\{Z\}$ begins to increase can be determined as approximately 72 Hz. Clearly this corresponds well to the behavior of the data shown in figure 3.

4.2. Case-hardened steel samples

A set of steel rods, 40 cm long and 11 mm in diameter, were used for the experiments. These were ground from half-inch diameter SAE/AISI 1045 steel; a type widely used for machined parts in the automobile industry. The centerless-grinding process used to grind the rods typically achieves

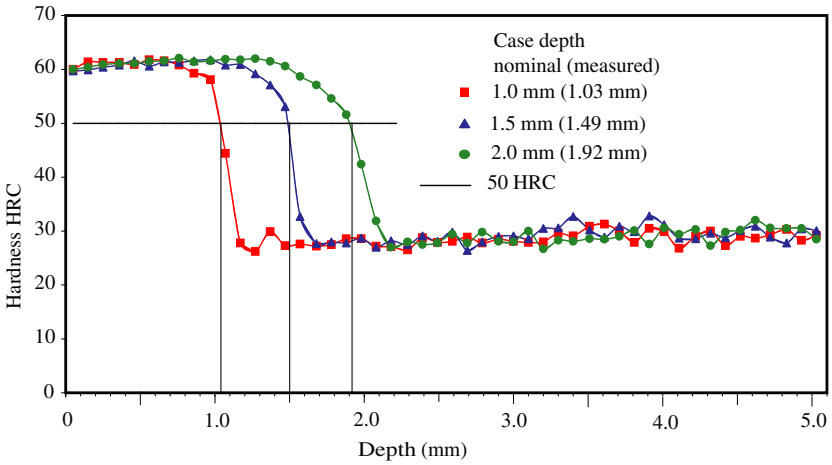

Figure 5. Variation of Rockwell C hardness with depth for a series of induction-hardened SAE/AISI 1045 cylindrical steel rods. The nominal case depths are 1.0, 1.5 and 2.0 mm. Actual measured effective case depths are 1.03, 1.49 and 1.90 mm. Effective case depth is measured at 50 HRC.

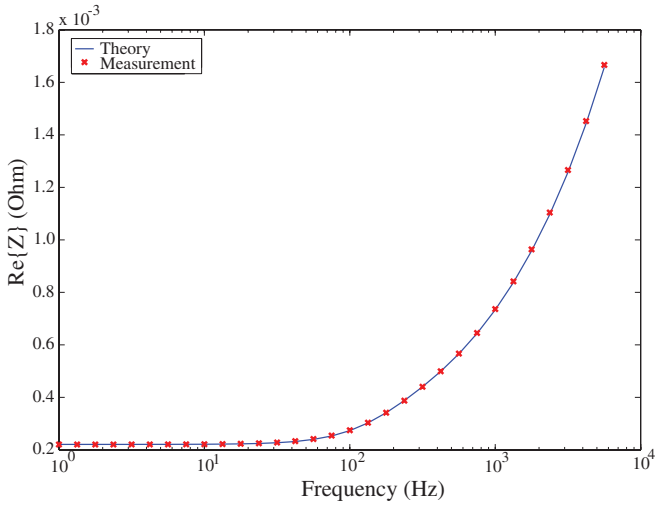

Figure 6. Comparison between theory and experiment of the real part of the impedance measured on a homogenous steel rod with conductivity fixed at 4.77 MS m^{-1} and relative permeability 65.6 determined by fitting multi-frequency ACPD data using the theoretical model.

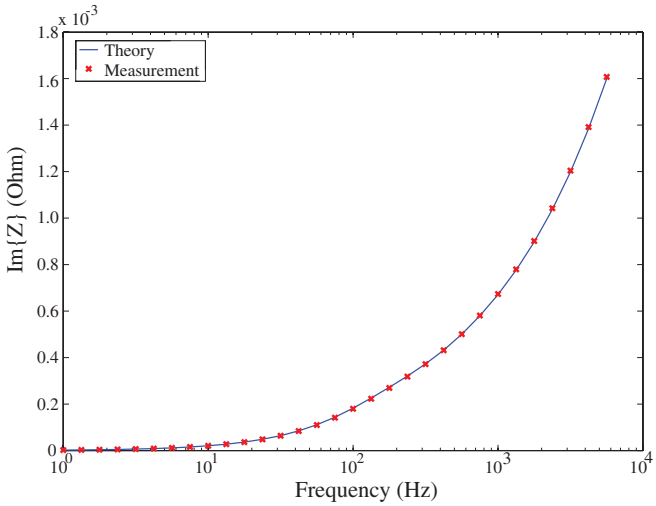

Figure 7. As for figure 6 but for the imaginary part of the impedance.

tolerance ± 0.01 mm. Induction hardening resulted in the hardness profiles shown in figure 5 for rods with nominal case depths 1.0, 1.5 and 2.0 mm. In the modeling it is assumed that the depth of case hardening does not vary along the length of the rods, or with rod orientation. Experimental tests indicate that variations in the depth of case hardening as a function of rod orientation are less significant than other sources of measurement noise. The rod parameters are also listed in table 1. Measurements were taken after the rod had been demagnetized. Demagnetization was achieved by mounting the rods concentrically inside a 48-cm-long solenoid with diameter 9 cm. The current flowing in the solenoid was reduced from a value high enough to nearly saturate the samples (approximately 8 A) to zero over a period of 62 cycles, at a frequency of 80 Hz. After demagnetization the residual surface magnetic induction field was checked to be below 3 G (3×10^{-4} T) using a hand-held gauss meter.

Table 1. Nominal and 50 HRC case depths of the samples studied.

Nominal case depth (mm)	Depth at HRC 50 (mm)
1.0	1.03 ± 0.02
1.5	1.49 ± 0.02
2	1.90 ± 0.02

4.3. ACPD measurement on untreated steel

Variation of the ACPD with frequency for an untreated rod of AISI 1045 steel is shown in figures 6 and 7. Fitting the conductivity and permeability is carried out by searching for values that minimize the penalty function $\mathcal{E}$ defined such that

$$\mathcal{E}^2 = \sum_i \frac{[Z^{\text{obs}}(\omega_i) - Z(\omega_i)]^2}{Z(\omega_i)^2}, \tag{30}$$

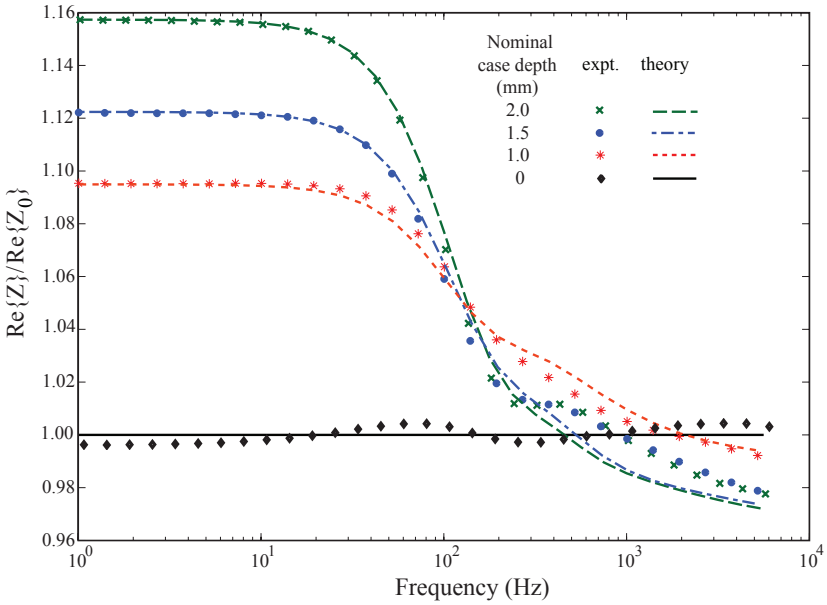

Figure 8. Resistance variation with frequency for three case-hardened steel SAE/AISI 1045 rods, normalized with respect to the theoretical untreated rod resistance.

Table 2. Conductivity, permeability and case-depth values found by optimizing the model fit, equation (28), to the experimental data. Although the fitting error for the hardened rods is less than 1%, the uncertainties quoted are determined on the basis of the 1% uncertainty in the fitted material parameters of the unhardened rod, which are used as values for the core parameters of the hardened rods, combined with the uncertainty in the separation of the pick-up pins.

Nominal case depth (mm)	Core σ (MS m^{-1})	Core relative μ	Case σ (MS m^{-1})	Case relative μ	Fitting error (%)	Estimated case depth (mm)
0	4.77 ± 0.08	66 ± 1	–	–	1	–
1.0	4.77 ± 0.08	66 ± 1	3.82 ± 0.06	50.6 ± 0.8	0.5	1.36 ± 0.02
1.5	4.77 ± 0.08	66 ± 1	3.87 ± 0.06	49.1 ± 0.8	0.3	1.91 ± 0.03
2	4.77 ± 0.08	66 ± 1	3.83 ± 0.06	48.5 ± 0.8	0.3	2.45 ± 0.04

where $Z^{\text{obs}}(\omega_i)$ represents a set of experimentally observed values and $Z(\omega_i)$ represents the corresponding theoretical predictions. Parameter estimates, obtained by averaging over 3 data sets using 20 frequencies in the range from 1 Hz to 6 kHz are shown in table 2.

The electrical conductivity for a longitudinal current in the soft steel rod was found to be 4.77 ± 0.08 MS m^{-1} and the relative permeability associated with the azimuthal magnetic field 66 ± 1. These uncertainties were estimated by combining the fitting error listed in table 2 with the uncertainty in the separation of the pick-up pins. Other uncertainties, such as that derived from variation in the rod diameter, are negligible compared with these two.

From equation (11) the value of the frequency at which Re$\{Z\}$ begins to increase can be determined as approximately 13 Hz, corresponding well with the behavior of the data shown in figure 6.

4.4. ACPD measurement on case-hardened steel samples

Assuming that the process of induction hardening does not significantly alter the conductivity and permeability of the substrate beneath the case-hardened layer, σ_1 and μ_1 are assigned the values determined for the untreated steel rod in section 4.3; $\sigma_1 = 4.77$ MS m^{-1} and $\mu_1 = 66$. With the substrate properties held fixed, and the self-inductance of the measurement circuit assumed to be the same as that determined in section 4.1, the electrical conductivity, permeability and case depth of the outer layer were adjusted to find an optimum least squares fit of ACPD model predictions, equation (28), to measurements using a numerical procedure[1]. This process of model-based determination of the material parameters and depth of the case-hardened layer was first tested on theoretically-generated data. Having found the required parameters, table 2, the theoretical fit can be compared with the experimental data as shown in figures 8 and 9. In these figures the results are normalized with respect to those for the untreated rod.

The numerical results show that the permeability and conductivity of the case-hardened layer, table 2, varies very little between specimens and both are somewhat lower than the corresponding values for the core material. A similar difference in material properties has also been observed in electromagnetic measurements on samples obtained by sectioning a case-hardened rod [13].

[1] Function 'lsqnonlin' in Matlab is used to find the best-fitting parameters.

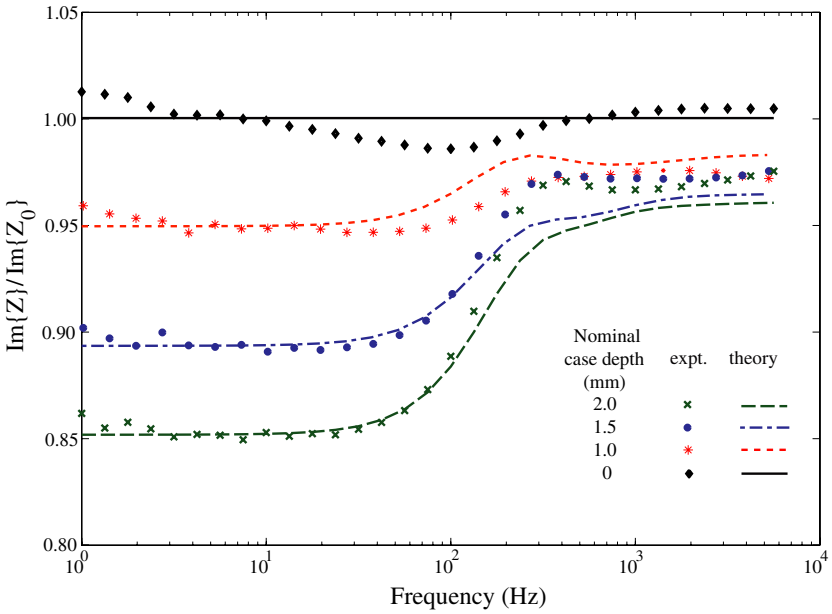

Figure 9. As in figure 8, but for reactance.

Comparisons between the theoretical calculations and the measurements in figures 8 and 9 show good agreement but this is hardly surprising since we have three free parameters. At low frequency, the real part of the normalized impedance indicates the overall resistance of the rod, which is increased compared with the untreated rod as a result of the case hardening. On the other hand, the overall permeability is decreased, as shown by the decrease in the imaginary part of the normalized impedance at low frequency. All curves show a transition region at about 100 Hz. The beginning of the transition, at about 10 Hz, corresponds approximately to the bounding frequency of the quasi-static region for the homogeneous steel rod, $f_s = 13$ Hz, calculated in section 4.3. We can deduce (although we do not show in detail here) that the frequency at which the transition in the data of figures 8 and 9 occurs depends on the parameters of the layered rod in a similar way to the dependence of f_s on the parameters of the homogeneous rod, equation (11). Indeed, test calculations indicate that the frequency at which the transition occurs becomes lower as the radius of the rod increases.

The real test of whether the model captures the physics of the measurement process is in the ability of the fitting process to reproduce the case depths found from destructive microhardness measurements. A comparison between the measured mid-hardness depth and that obtained by modeling is shown in figure 10. It is found that the nondestructive estimates of case depth exceed those obtained from Rockwell C hardness measurement (at 50 HRC) by about 30%. This is somewhat larger than might be required for an accurate inspection technique. However, an engineering solution could use a linear correction factor to reduce the error. One source of the discrepancy is that the Rockwell C criterion for depth means that it occurs near the top of the hardness curve in the initial part of the transition region whereas the electromagnetic measurements attempt to locate the transition region in a more unbiased way. In addition, there is evidence in the literature

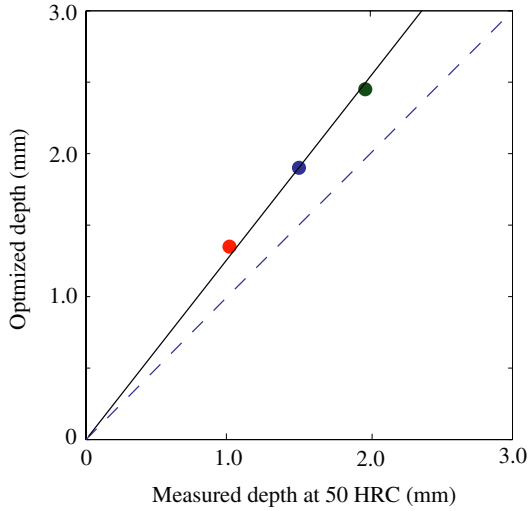

Figure 10. Case depth determined by optimizing parameters to obtain the best fit between ACPD measurements and theoretical values, equation (28), compared with values found using an indenter on a section of each specimen at 50 HRC (Rockwell hardness).

that the transition in the permeability from its core- to surface-value occurs at a greater depth than the hardness transition, by approximately 15% [13]. A similar, but lesser, effect is observed in the conductivity transition [13]. This implies that we might expect the case depth predicted by a nondestructive electromagnetic technique, such as this one, to be greater than that measured directly. Another source of error is the assumption in the model that σ and μ change abruptly at the interface between the case-hardened layer and the substrate. From figure 5 it is clear that the hardness transition has a non-negligible length, that increases as the depth of hardening increases. Indeed, this difficulty is exacerbated in steel that is hardened by carburization, in which the hardness transition is significantly broader than that in the induction-hardened parts

studied here. The profile of the broad transitions could in principle be modeled by means of an error function or similar, but further complexity in the model has the effect of increasing the number of free parameters.

5. Conclusion

An ACPD measurement model has been used to determine the conductivity and relative permeability of homogenous metal rods. A generalized ACPD theory has been developed for a layered rod, and used in the determination of depth, electrical conductivity and the permeability of a case-hardened surface layer. The case depths found in this way over-predict those measured destructively by approximately 30%. Simplifications in the model, such as the assumption that σ and μ change abruptly and coincidentally with the depth of case hardening, may give rise to this discrepancy. In addition, the depth at which permeability changes from its core- to surface-value has been observed to be greater than the depth of the hardness transition by approximately 15% in a 50 mm diameter steel rod induction-hardened to approximately 16 mm [13].

The measurement system used in this study is not intended as a practical solution to the problem of monitoring case-hardened steel components in a manufacturing environment. Instead, it serves to establish the feasibility of finding case depth using ac potential-drop measurements. The results suggest that a model-based approach using multi-frequency four-point ACPD could satisfy an industrial need for nondestructive measurement of case depth that does not require the use of calibration samples. Potential-drop measurements made using four spring-loaded contacts have shown that the conductivity of metal plates can be determined more accurately with the ACPD technique than with eddy-current measurements [14], mainly because the probe is easy to characterize accurately [15]. Also, measurements can be carried out on a relatively small region of the material surface, e.g. less than 1 cm in length. Use of an eddy-current encircling coil to determine the depth of case hardening is less sensitive than ACPD because the eddy-current probe impedance varies approximately with the ratio σ/μ in the material over the usual operating frequency range of most eddy-current probes. In table 2 it is seen that the ratio of these material parameters is very similar in the core (0.072) and the case-hardened layer (0.076) of the rods under test. In the ACPD measurements, however, these parameters are clearly distinguished (equations (6) and (10)), leading to better measurement sensitivity to their variation with depth.

In future work, existing models of four-point ACPD measurements on flat surfaces [15–17] will be adapted to deal with curved surfaces, such as that of a crank shaft bearing.

Acknowledgments

This work was supported by the NSF Industry/University Cooperative Research program. The authors thank D A Rebinsky, Caterpillar, Inc., Technical Center, Peoria, IL for providing samples and case-depth data, and M J Johnson for advice on the experiments.

References

[1] Bochenin V I and Kuznetsov V P 2004 A radioisotopic method for measuring the depth of surface hardening of oil-and-gas pipelines *Russ. J. NDT* **40** 808–10

[2] Xiang D, Hsu N N and Blessing G V 2000 Case hardening measurement with quantitative surface acoustic microscopy *AIP Conf. Proc.* **509** 1471–8

[3] Johnson W, Kim S A and Norton S J 2005 Profile of material properties in induction hardened steel determined through inversion of resonant acoustic measurements *Review of Progress in Quantitative NDE* vol 24B ed D O Thompson and D E Chimenti (New York: Plenum) pp 1285–91

[4] Mandelis A 2002 Go where no light has gone before *Opt. Photon. News* **6** 32–7

[5] Liu Y, Baddour N and Mandelis A 2003 *J. Appl. Phys.* **94** 5543–8

[6] Takeo F, Nakajima K, Baba T, Aonahata Y and Saka M 2004 Arrangement of probes for measuring case depth by means of four-point probes *Key Eng. Mater.* **270–273** 82–8

[7] Makarov A V, Kogan L Kh, Gorkunov E S and Kolobylin Yu M 2001 Eddy-current evaluation of wear resistance of case-hardened chromium-nickel 20KhN3A steel *Russ. J. NDT* **37** 136–44
Translated from Makarov A V, Kogan L Kh, Gorkunov E S and Kolobylin Yu M 2001 *Defektoskopiya* **2** 67–78

[8] Kai Y, Tsuchida Y and Enokizono M 2005 Nondestructive evaluation of case hardening by measuring magnetic properties *Electromagetic Nondestructive Evaluation (IX)* ed L Udpa and N Bowler (Amsterdam: IOS Press) pp 143–50

[9] Zhu B, Johnson M J and Jiles D C 2000 Evaluation of wear-induced material loss in case-hardened steel using magnetic Barkhausen emission measurement *IEEE Trans. Mag.* **36** 3602–4

[10] Theiner W A, Bucher B, Kern R, Kröning M, Meyer R and Wolf H 1996 Process integrated nondestructive testing for evaluation of hardness *Proc. 14th World Conf. on NDT* pp 573–6

[11] Alpeter I and Kröning M 1994 Nondestructive determination of the hardening depth in inductive hardened steels *Nondestructive Characterization of Materials* vol 6 (New York: Plenum) pp 659–68

[12] Abramowitz M and Stegun I A (ed) 1972 *Handbook of Mathematical Functions with Formulas, Graphs, and Mathematical Tables* (New York: Dover) equation (11.3.24)

[13] Johnson M, Lo C, Hentscher S and Kinser E 2005 *Electromagetic Nondestructive Evaluation (IX)* ed L Udpa and N Bowler (Amsterdam: IOS Press) pp 135–42

[14] Bowler N and Huang Y 2005 Electrical conductivity measurement of metal plates using broadband eddy-current and four-point methods *Meas. Sci. Technol.* **16** 2193–200

[15] Bowler N and Huang Y 2005 Model-based characterization of homogeneous metal plates by four-point alternating current potential drop measurements *IEEE Trans. Mag.* **41** 2102–10

[16] Bowler N 2006 Theory of four-point alternating current potential drop measurements on a metal half-space *J. Phys. D: Appl. Phys.* **39** 584–9

[17] Bowler J R and Bowler N 2007 Theory of four-point alternating current potential drop measurements on conductive plates *Proc. R. Soc.* **463** 817–36